

An Image Analysis-Based Approach for Automated Counting of Cancer Cell Nuclei in Tissue Sections

Constantinos G. Loukas,^{1,2*} George D. Wilson,¹ Borivoj Vojnovic,¹ and Alf Linney²

¹Gray Cancer Institute, Mount Vernon Hospital, Northwood, Middlesex, United Kingdom

²Department of Medical Physics and Bioengineering, University College London, Shropshire House, London, United Kingdom

Received 12 November 2002; Revision Received 13 March 2003; Accepted 11 April 2003

Background: Semiquantitative evaluation and manual cell counting are the commonly used procedures to assess positive staining of molecular markers in tissue sections. Manual counting is also a laborious task in which consistent objectivity is difficult to achieve. Recently, image analysis has been explored, but the studies reported were limited to histological images acquired at high magnification and containing uniformly stained cells.

Methods: The analyzed material consisted of histological sections from different squamous cell cancers that had stained for proliferation using Ki-67 and cyclin A detection. The first step of the method was based on detecting the overall number of cells irrespective to their stain, using second-order edge detection methodology. Then proliferating cells were located using principal component analysis (PCA) of the color image, combined with histogram thresholding.

Results: The algorithms' performances were validated on tissue section images encountered in routine clinical prac-

tice by comparison with objective measures of performance and manual cell identification. The algorithms correlated closely with manual counting of all cells ($r^2 = 0.96-0.97$) and stained cells (4–7% cell count error).

Conclusions: Cell counting in complex large-scale histological images could be applied in routine practice using edge and color information. The proposed technique provides several benefits, such as speed of analysis, consistency, and automation. Moreover, it is faster than human observation and could replace the laborious task of manual cell counting. *Cytometry Part A 55A:30–42, 2003.*

© 2003 Wiley-Liss, Inc.

Key terms: image analysis; histology; segmentation; cell counting; edge detection; thresholding; principal component analysis

Cancer prognosis and cancer cell detection are critical issues for clinicians. Since the early 1970s computer-assisted image analysis started to contribute significantly toward the solution of these problems, particularly in the field of cytology automation. Considerable effort was devoted to the analysis of images of blood cells (1), and cervical smears (2), as well as to the development of expert systems for automated cytodiagnostics (3). The overall effort and the degree of success were restricted though, in a large part due to the simplicity of the images themselves, usually containing a few isolated cells against a plain background.

The research in automating the analysis of cytological specimens was the main drive for exploring similar, but rather more challenging, areas such as histology. The detection of cellular structures or cell counting is a very common task, which in histological preparations containing histological noise, such as debris and synthetic materials, is arduous to automate using standard image analysis tools. In addition, manual cell counting is a laborious task

suffering from subjectivity and an inability to derive more complex information (e.g., stain distributions, geometric relationships to other important structures such as vascular networks).

The interest in measurements in tissue sections has been boosted by the increase in computational power of modern computer systems, allowing automated performance of tasks that were otherwise executed manually. Several investigators have applied thresholding in order to implement cell counting in tissue section images. These

Contract grant sponsor: Cancer Research UK (formerly Cancer Research Campaign); Contract grant numbers: SP219510202, SP2195/003; Contract grant sponsor: Cancer Research Campaign; Contract grant number: STU 045/001.

*Correspondence to: C. Loukas, Sobell Department of Motor Neuroscience and Movement Disorders, Institute of Neurology, Queen Square, London WC1N 3BG, UK.

E-mail: c.loukas@ion.ucl.ac.uk

Published online in Wiley InterScience (www.interscience.wiley.com). DOI: 10.1002/cyto.a.10060

methods can help to reduce manual data recording and user error. Semiautomated systems have been developed to count pixels in spatial regions specified by the user (4), or within thresholds set interactively (5), while other investigators have experimented in the color domain (6). More sophisticated approaches have used multistage segmentation based on statistical models, and exhibited their potential to overcome many of the limitations of previously existing methods, but these were demonstrated in small-scale images containing fairly circular and uniformly stained nuclei (7). More recently, artificial neural network (ANN) methods have also made some contribution, although reporting a limited degree of accuracy and high computational overhead (8). Yet, most of the published studies lack the implementation of formal validation experiments and/or comparison with expert-generated results.

Although a variety of segmentation algorithms have been developed over the past several years, the problem of cell nuclei segmentation is still central, and thus an important subject in the study of automated histology. The primary aim of this research study was to develop a fast, and easily applicable in routine practice by histologists, method for detecting several hundreds of cell nuclei in large-scale histological images. This would also strengthen the currently employed semiquantitative and tedious examination, by visual inspection, of the histological material. Specifically, we have used a multistage algorithm that focuses on the detection, firstly of the overall number of cells irrespective to their stain, using edge detection, and secondly of the number of proliferating cells, using principal component analysis (PCA). Then the histogram of the output image is processed for producing a binary image. Following extraction of the required features, standard morphological operations are utilized to define the regions of interest, whereas recognition of touching or overlapping cells is performed using a distance map transformation.

MATERIALS AND METHODS

Immunohistochemical Staining of Sections

The material studied consisted of histological sections from different squamous cell carcinomas of the head and neck region. The tumors originated from a variety of sites within the head and neck and displayed variation in their differentiation status. The tumor material had been processed through standard procedures, embedded in paraffin blocks, and 4- μ m sections cut for immunohistochemistry. The material was stained using standard procedures, described elsewhere (9), for Ki-67 or cyclin A proliferation markers. Mayer's hematoxylin was used for counterstaining cell nuclei in blue, while the antigens were visualized by brown staining with diaminobenzidine.

Image Analysis Hardware and Software

The tissue section images were captured using a Zeiss Axioscop transillumination microscope, coupled to a JVC

KY55F 1/3-inch (6.4 \times 4.8 mm) 3-CCD color camera. The image acquisition software was an in-house-developed module added to Visilog version 5.02 (Noesis S.A., Les Ulis Cedex, France). The resolution of the images captured was 768 \times 576 pixels, and they were saved in a TIF (tagged image file) format. The captured images were digitized using a Matrox Meteor™ frame grabber, installed in a PCI bus 600-MHz Pentium™ PC. A \times 40 objective ($NA_{obj} = 0.75$, $NA_{condenser} = 0.5$, resolving power (Rayleigh) $d = 0.49 \mu\text{m}$ at $\lambda = 500 \text{ nm}$) was used during acquisition, providing a compromise between adequate resolution and maximum field of view of the regions of interest, depending on the particular task under investigation. The pixel size, at the object plane (230 \times 173 μm^2) was 0.3 \times 0.3 μm . Prior to processing, all images were examined for shade correction. The entire image processing algorithms and software reported here were developed in the C programming language, using the LabWindows®/CVI™ 5.5 (National Instruments Corporation, Austin, Texas) libraries.

Cell Counting Using Second-Order Edge Detection

Many algorithms have been developed to segment images using edge detection (10). One of the approaches presented in this paper utilizes second-derivative edge detection based on identifying the generated zero crossings. This approach was investigated because of the requirement for an automated method readily applicable in a series of images from a whole tissue section, with minimum interaction from the histologists and a great degree of accuracy. The *Laplacian of Gaussian* (LoG) edge detector (11) has the advantage of smoothing prior to edge detection (crucial in noisy histological material), and its zero-crossing response when an edge is encountered enhances its effectiveness.

The concept behind LoG is based on convolving an image with the Laplacian of a 2D Gaussian (G) function, that is, a rotationally symmetric convolution filter:

$$LoG(x, y) = \nabla^2 G(x, y) = A \left(2 - \frac{x^2 + y^2}{\sigma^2} \right) e^{-(x^2 + y^2)/2\sigma^2} \quad (1)$$

where A is simply a constant used to regulate the magnitude of the Gaussian, σ is the standard deviation determining its spatial scale, and x, y are the 2D spatial coordinates of the image.

Although the LoG filter provides a promising tool, like all second-order edge detectors it should be followed by a zero-crossings procedure that detects local edgels (i.e., edge elements), which are generally unconnected. As will be shown in the experimental section, due to the large number of cells and histological noise present in the images, LoG was found to produce excessive edge responses that were impossible to link and thus form meaningful objects.

The previous observations led to the idea of modifying the LoG in order to tackle the problem of nuclear edgel

linking. The first attempt was based on applying a negative threshold, instead of a zero-crossing routine, following edge detection. The intention was to detect all negative second-order variations that are caused whenever an edge is present (due to the transition of gray-level intensity from the histological background to nuclear boundaries), enabling localization of thick internal boundaries around the cells.

However, since the LoG is mainly designed to generate a zero crossing and not a negative value where an edge is present, it was observed to produce some false responses that corresponded to negative variations other than those generated from the edges of the cell nuclei (mainly due to histological noise). Thus, the entire LoG filter was shifted downward in such a way that its shape was retained intact, generating a zero response when assimilated with a field of constant gray levels. The new modified version of LoG was named OLGA, which is an acronym for Optimum Laplacian of Gaussian Assimilator (12):

$$\begin{aligned} OLGA &= LoG - A' e^{-[(x^2 + y^2)/2\sigma^2]} \\ &= A \left(K - \frac{x^2 + y^2}{\sigma^2} \right) e^{(x^2 + y^2)/2\sigma^2} \quad (2) \end{aligned}$$

where $K = 2 - A'/A$ is a factor used to shift downward the entire LoG. This procedure achieved the condition: $\sum Z_i < 0$, where the Z_i values are now the coefficients of OLGA, which is configured as a 2D kernel operator. However, the new central pixel value of OLGA is now given by $Z_{0\ new} = Z_0 + |\sum Z_i|$, where $Z_0 = A \cdot K$, so that $\sum Z_{i\ new} = 0$, and thus the filter's response is zero whenever convolved with a constant gray-level neighborhood. A 1D profile of the OLGA obtained from a LoG with $\sigma = 4$ and using $K = 0.7$, $A = 1$, is shown in Figure 1a. A 2D configuration of this kernel (i.e., square matrix of size 8.5σ , as suggested in Huertas and Medioni (13)), was used for the cell nuclei detection, providing a reasonable compromise between more cellular edge features and fewer nonmeaningful details. OLGA may be considered a combination of a Laplacian filter (i.e., large positive central pixel value with most outer coefficients negative) and a LoG that provides greater smoothing due to the Gaussian tail. This combination helped to enhance the nuclear boundaries, but at the same time, using the features of LoG, to suppress the unwanted effect of responding to image discontinuities that corresponded to noise, rather than real edges (see also Fig. 1b and c, discussed in the Results section).

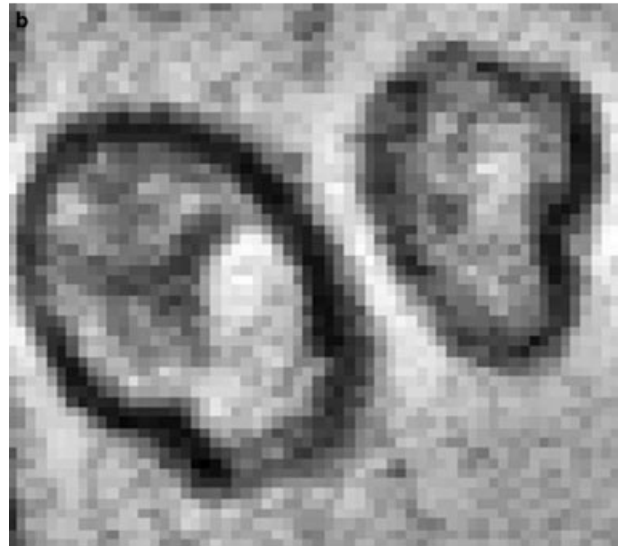
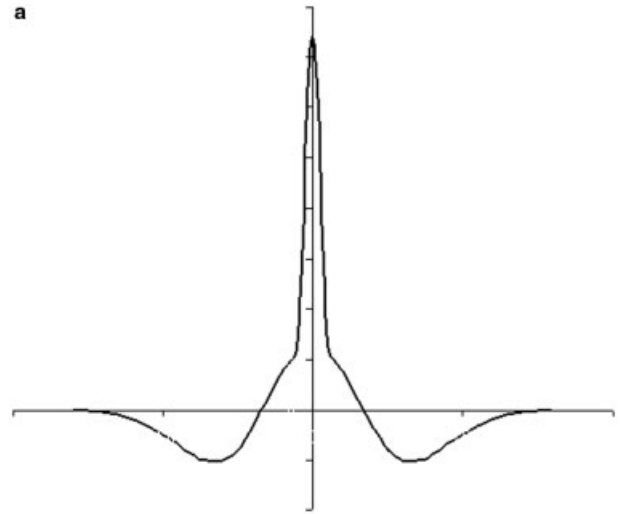


FIG. 1. **a:** A 1D profile of OLGA ($\sigma = 4$, size = 33×33). **b:** A 2D configuration of this operator was used for detecting the overall number of cells, irrespective to their stain, in the histological images tested. **c:** A sample image of two cell nuclei. **c:** The pattern of thick cell nuclei borders detected after applying a negative threshold on the OLGA output image. Note that OLGA essentially transforms the gray values of the pixels located in the cell border to negative, so that they can be detected readily with thresholding.

Morphology and Distance Mapping

After edge detection the boundaries of the cell nuclei are defined in the binary image, but some noncellular particles are also present. The binary image is thus further processed to remove objects that do not correspond to nuclei by successively applying the following morphological operations: *region filling* for achieving solid particles, *low-pass filter* for removing small artifacts, and *opening* for smoothing cell boundaries.

In the final binary image some cell nuclei formed clusters of overlapping or touching cells. A further procedure was thus applied before counting. An implementation of *Euclidian distance mapping* (14) was tried, followed by identification, using nonmaxima suppression, of the individual centers. Nonmaxima suppression serves the purpose of retaining only maxima in the distance map of the image, while no local maxima are removed. However, while this approach is preferred for objects of a regular shape, in the present application a simpler method was found to be more effective (15,16). By successively eroding the binary image, A (using a standard 3×3 kernel operator), a new *distance map* image, DM, was derived by encoding the pixel value of each particle as a function of the pixel's distance to the object's border according to the formula

$$DM_i = (A - i \times \text{Erode}(A)) - \sum_{j=1}^{i-1} DM_j \quad (3)$$

where $DM_1 = (A - \text{Erode}(A))$, DM_i is the distance map zone at the i th step, and $i = 2, \dots, N$. N is the maximum number of erosions until $DM_N \neq \emptyset$.

DM_i is given essentially an increasing integer value, which is successively assigned to the pixels eroded at each iterative step. For example, DM_1 is assigned the initial value of 1 and corresponds to a one-pixel width zone, surrounded by the detected object's external border. Thus, these distance map zones represent an attached group of pixels having a different distance from the cell border, depending on the erosion step each time the binary image was eroded. The pixels having the maximum distance to the nucleus border can then be detected using nonmaxima suppression.

Segmentation of Labeled Cell Nuclei

The second phase of this multistage algorithm was to segment those cells having stained for a proliferation marker. An automated algorithm based on PCA of color images was implemented in conjunction with several widely used threshold selection techniques applied for comparison.

The PCA Algorithm

When applied to color images, PCA generates weighted linear combinations that may adapt to the spectral changes of the cells being imaged. In a few studies

(17,18), this adjustment was done manually, which is a time-consuming proposition, involving manual and usually inaccurate modification of the weights from one image to another. PCA has also been applied successfully for the enhancement of images of stained cervical smears (19). However, that approach was implemented semiautomatically and applied in relatively simple images at high magnification showing fairly uniform-stained structures. The main objective here was to apply a similar technique but automatically, in more complex and larger-scale images, while processing further the resulting image to extract the nuclei of interest. In principle, PCA identifies a linear transformation of the original color coordinate system such that the three axes of the new coordinate system coincide with the directions of the largest spreads of the point distribution (20):

$$I(x, y) = w_1R(x, y) + w_2G(x, y) + w_3B(x, y) \quad (4)$$

where the w_i values are the computed weights during PCA, I is the output image, and R , G , and B denote the images in the red, green, and blue spectral bands, respectively. As will be presented in the Results section, images generated by the first principal component (1st PC) present the best contrast showing the stained cells greatly enhanced over all other structures.

Histogram Processing

In the few occasions where standard thresholding methods failed (21-24) (see also "Evaluation of PCA" in the Results section), the histogram of the 1st PC was further processed in order to set an appropriate threshold for detecting the proliferation-labeled cell nuclei using a different criterion. This was essentially based on the prior knowledge that proliferating cells appear with light gray values in the 1st PC, and thus pixels having gray values close to 255 are most likely to belong to these cells. Hence, in this case the histogram was searched backwards, starting from 255, for thresholding the image, until a termination criterion was fulfilled. The termination criterion was that the percentage difference between the numbers of pixels with gray-level equal to i and $i - 1$ should not exceed a predetermined fraction (usually set to 0.1) of the difference between maximum and minimum gray levels in the entire image, as a measure of contrast. This is basically an analytical rule that provides a fixed maximum value for the rate of increase in number of pixels as the major peak of the histogram, which represents structures not of interest, is approached.

RESULTS

Evaluation of Edge Detection Methodology

This section provides the results obtained after applying LoG and OLGA to a series of tissue section images with variable staining quality. For comparison, two more algorithms were implemented: Laplacian and the Canny edge

detector, as both have been employed in the past for similar segmentation problems (25–27). The first is essentially equivalent to applying directly a second-order derivative operator without any preprocessing (20) (as opposed to LoG), whereas the second is a very common edge detection filter, used widely in the machine vision domain for segmentation purposes (see Canny (28)).

Figure 2a shows a small portion of a tissue section image containing cell nuclei of various shapes due to different cutting angles of the section, many of which are clustered, making their identification a nontrivial task. The brown cells were stained using a proliferation marker. However, at this stage the main interest was to detect all cellular structures present in the image, irrespective to the stain used to mark them. For the sake of clarity, only the first quarter of the original image is shown here. Figure 2b–d illustrate the output images using the Laplacian, LoG, and Canny edge detectors, respectively. For this implementation the color component exhibiting the best contrast between nuclei and background was chosen as the input to each edge finder (usually the red component). It is clear that after searching for zero crossings in the filtered image, all algorithms generated a fuzzy set of edgels, which were extremely difficult to connect, resulting in incorrect segmentation. The Laplacian operator had the worst performance, generating numerous false edgels, something that was expected due to its unacceptable sensitivity to noise. LoG produced superior results, but some edges were also significantly deformed and very difficult to link. The Canny edge detector provided the least number of false responses, but on the other hand, it failed to mark all real edges. Figure 2e provides the output of the modified LoG filter (referred to here as OLGA), which seems to combine both greater noise suppression and lower edge deformation. Figure 2f is essentially equivalent to Figure 2e superimposed on the original image Figure 2a.

To obtain a better understanding on how OLGA works, by generating a pattern of thick edgels around each nucleus, Figure 1b shows a sample image containing only two cell nuclei where the hematoxylin stain has been absorbed more intensively by their border. This image was also enhanced further for better visualization purposes. To segment the nuclei by detecting their border, it is vital to apply an edge detection technique capable of tracking those low-intensity (i.e., black) pixels located in the cellular border. Figure 1c shows the output after applying OLGA with $\sigma = 4$, and then using a negative threshold in order to detect a pattern of thick boundaries. The borders detected through this procedure have a width of several pixels, and thus they could easily constitute the actual cellular objects of interest using some binary image processing, and without any need to perform edgel linking, as opposed to LoG.

Figure 3a–d illustrates some examples of automated counting performed on large-scale histological images from different tumors and with different stains (brown cells were stained with either of the proliferation mark-

ers Ki-67 or cyclin A, whereas blue cells were stained with hematoxylin). The borders of the cells detected by OLGA are marked with red, whereas the centers of clustered nuclei found by the process of repeated erosions are shown in yellow. Staining quality is variable, resulting in some cell nuclei being stained weakly, making the detection of their border a challenging task. Note also that the sizes and shapes of the cellular objects are also variable and irregular, due to different cutting angles of the tissue. All images studied contained a very large number of cells, usually greater than 300. At this point it should be mentioned that before counting, an idea similar to a size filter was invoked (pixel distance, ≤ 4 erosions) for ignoring any small objects that are unlikely to be cell nuclei.

From the output images, it is clear that cell nuclei are detected robustly, including those that touch or overlap one another. A more quantitative evaluation is presented in the next two sections, which contain two different sets of rather formal validation experiments.

Quantitative Evaluation of Cell Nuclei Edge Detection

In many, if not most, applications in which edge detection is performed in order to outline objects in a real scene, the only performance measure of ultimate importance is how well edge detector markings match the visual perception of object boundaries. Thus, an attempt was made to compare more quantitatively the algorithms studied. A very common approach employed in this situation is based on the figure of merit (FOM) (29). Several other researchers have employed this method over the years, and for various applications (30,31). Basically, the FOM for edge detection is defined as

$$FOM = \frac{1}{N} \sum_{i=1}^N \frac{1}{1 + \alpha d^2(i)} \quad (5)$$

where $N = \max\{I_I, I_A\}$, I_A is the number of edge pixels found by the edge detector (actual edges), I_I is the ideal number of edge pixels in the test image, and the function $d(i)$ is the nearest distance between the ideal i th edgel and the one found by the edge detector. The parameter α is a scaling constant and should be set constant (~ 0.8) for any set of trials.

This metric is essentially a function of the distance between correct and measured edge positions. To calculate such a measure, the positions of the true edge pixels need to be known. As a reasonable approximation, the cell edges outlined by an independent observer were used as the gold standard. Furthermore, to simulate conditions of low, medium, and high noise, FOM was measured after independent Gaussian noise of three different standard deviations: $\sigma_1 = 3$, $\sigma_2 = 6$, and $\sigma_3 = 9$ were added to the original gray-level images.

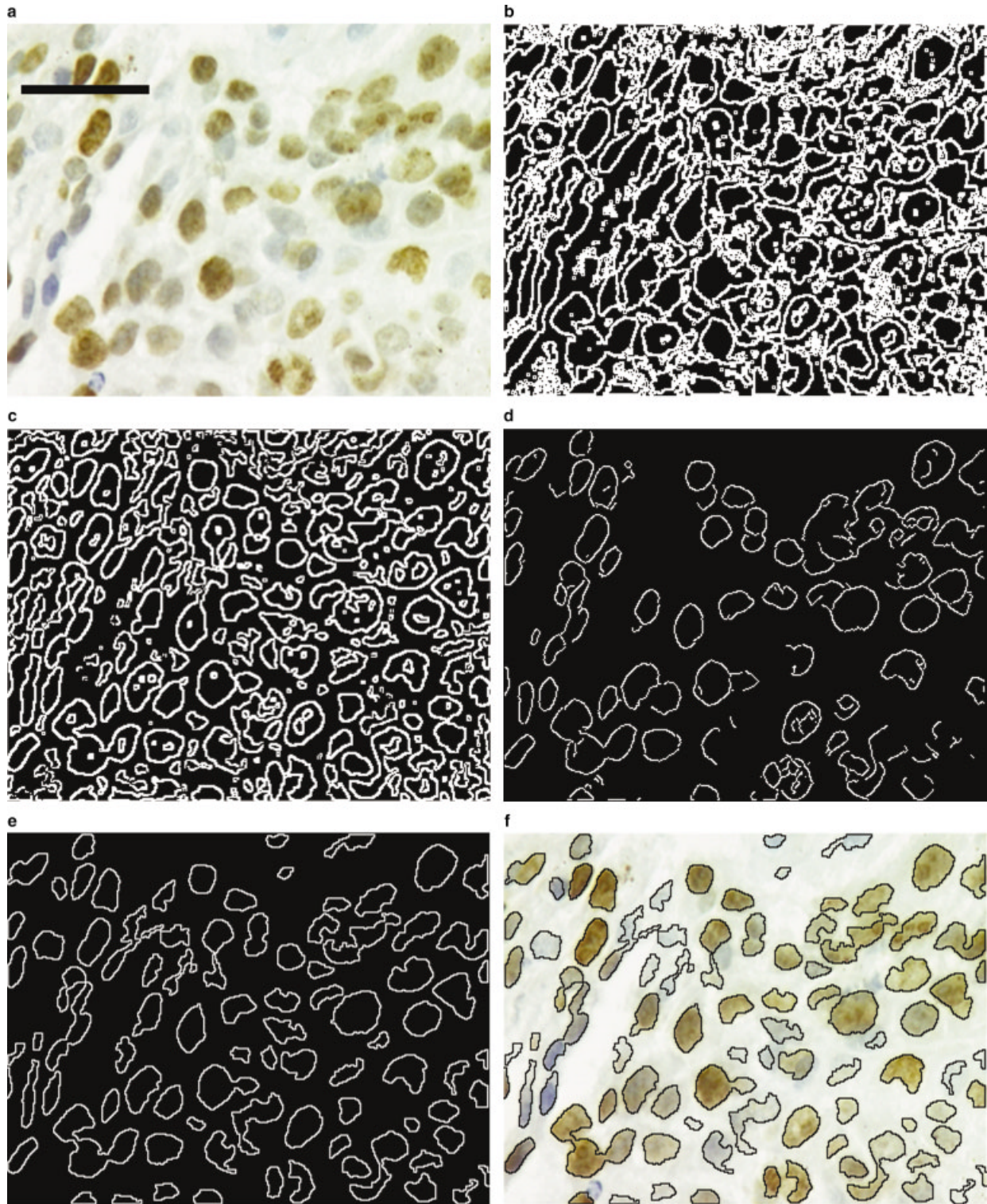


FIG. 2. **a**: A portion of a histological image (approximately one quarter of the full-scale image). **b-e**: The output image after applying the Laplacian filter (b), LoG (c), the Canny edge detector (d), and OLGA (e) (after hole-filling the OLGA output). **f**: After superimposing the OLGA segmented image (e) on the original color image (a). Bar = approximately 30 μm .

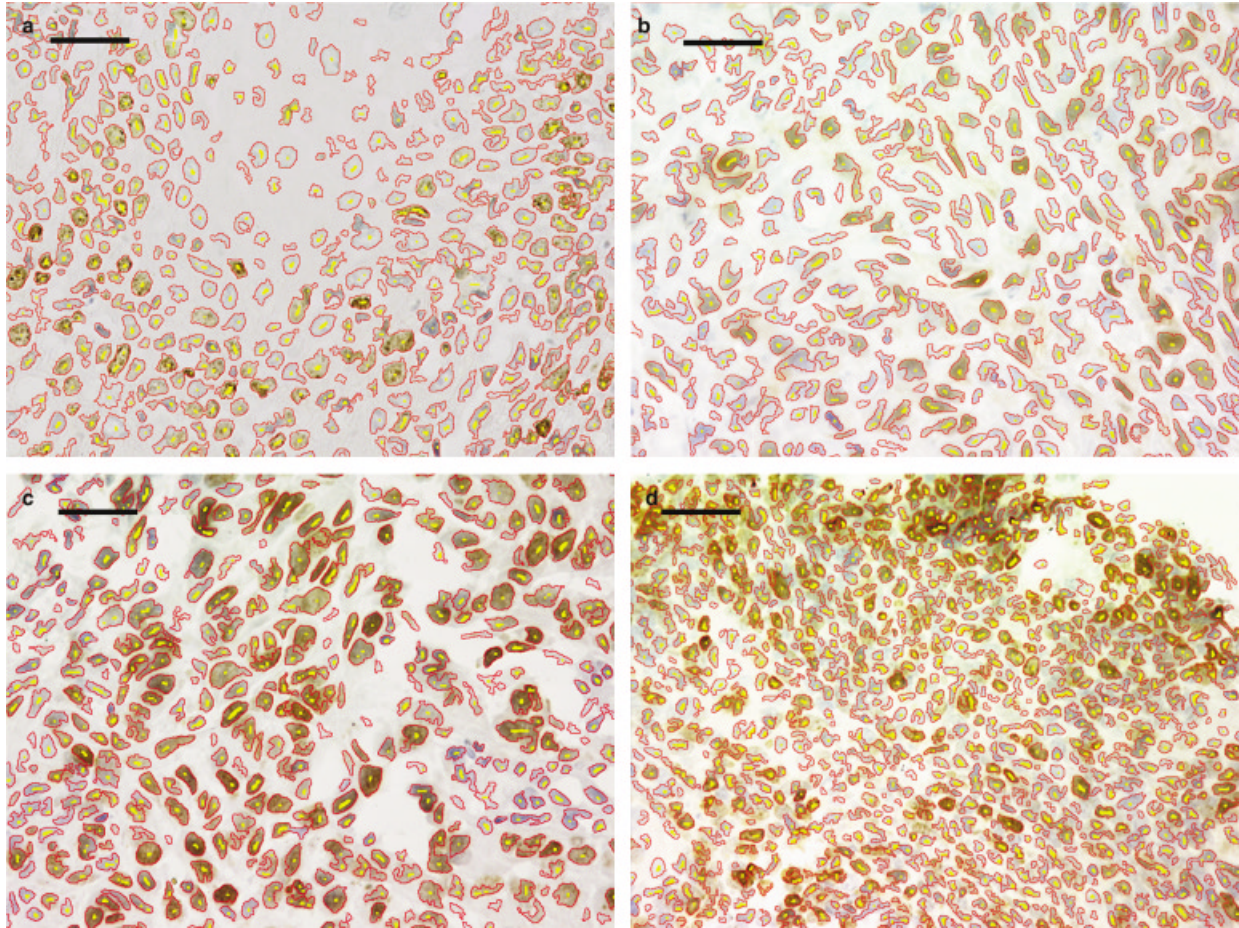


Fig. 3. Four typical examples of large-scale histological images of squamous cell carcinoma of the oral cavity, containing 328 (a), 274 (b), 322 (c), and 761 (d) cells, respectively. OLGA was applied with $\sigma = 4$. Cell nuclei borders are marked with red, whereas their centers are shown in yellow, denoting the presence of clustered/overlapping nuclei when a red border encloses more than one yellow spot. Bar = approximately 30 μm .

Figure 4 shows plots of the FOM (average values over 20 test images) as a function of noise level for LoG, Canny, and OLGA. The Laplacian filter was excluded from this experiment because it resulted in an ex-

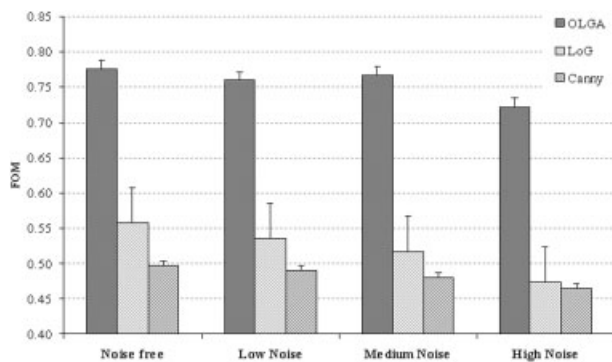


Fig. 4. Comparison results of three different edge detection algorithms (LoG, Canny, and OLGA) at presence of noise of various levels (i.e., $\sigma = 0$, $\sigma = 3$, $\sigma = 6$, and $\sigma = 9$). Vertical axis corresponds to an average value of the FOM over 20 test images.

remely fuzzy pattern of edgels for all test images studied. From the graph plotted it can be seen that predictably the performance of all methods deteriorates as the signal-to-noise ratio (SNR) decreases. OLGA had the best performance by far, whereas its FOM is almost constant, indicating a high degree of stability and tolerance in the presence of noise.

Comparison of OLGA with Manual Counting of Cell Nuclei

A more direct evaluation of OLGA involved comparison between image analysis and human observer cell counting. Specifically, a test set of 15 full-scale histological images with variable staining quality was selected. Each of the histological images was counted using OLGA in the outset, followed by the appropriate morphological operations described previously for detecting clustered cells.

Figure 5 shows the scatter plots containing the blinded counts between the two different observers and those generated by image analysis. For comparison, the counts produced by the two experts are also plotted in the same figure. The lines in the graphs represent linear regression

curves, whereas the correlation data obtained from the analysis are shown in Table 1. From Table 1 it can be seen that correlation coefficients, relating the computer-generated and manual cell counts, are highly significant and comparable to that found between the two observers. The coefficients of the linear regression curves show that OLGA tends to overestimate the number of cells, in relation to the counts found by either of the two observers, by 20–30 counts per image. However, this has little effect on the final outcome, if one considers that the average number of cells per image was 400; i.e., this represents an error of about 5–8%, which is slightly higher than the error rate associated with interobserver variability (approximately 5%).

Evaluation of PCA

Figure 6a shows a typical large-scale histological image containing proliferating cells stained differently than the others. This may be considered as an example of a tissue image with average staining quality, containing background noise in the form of cellular debris, histological variations, and many heterogeneously stained cell nuclei. The histograms of its three color bands are shown in Figure 6b, where it can be concluded that all of them are characterized by a prominent broad peak close to the right side (i.e., 255), corresponding essentially to the histological background and hematoxylin-labeled nuclei.

Among the three new images generated by PCA, the 1st PC (Fig. 6c) presents the best contrast, showing the proliferating cells greatly enhanced over all other structures. This is also clear from its histogram (Fig. 6d), which exhibits a bimodal shape, having two peaks. The right peak, corresponding in reality to the proliferating nuclei, is very well separated, and thus a threshold value may be readily applied using standard threshold selection algo-

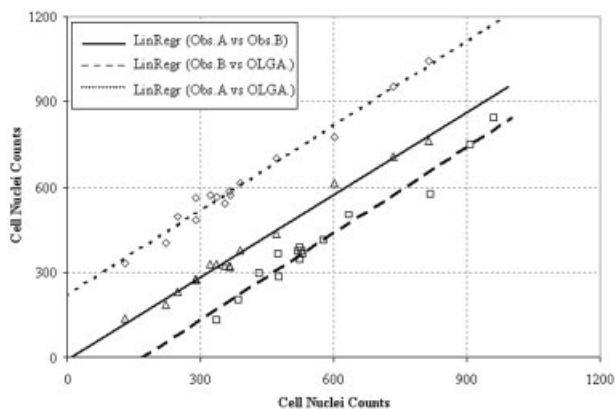


FIG. 5. Scatter plots between the cell counts found by two different observers and the OLGA-based algorithm, in 15 histological images. The linear regression data of the plotted lines are shown in Table 1. Note that a vertical offset of +200 and -200 nuclei were used for Lin.Regr. (Obs.A versus OLGA) and Lin.Regr. (Obs.B versus OLGA), respectively, without which both lines would almost coincide with the middle Lin.Regr. (Obs.A versus Obs.B).

Table 1
Linear Regression Results Obtained From Validation Studies on 15 Large-Scale Histological Images Containing a Range of 129 to 844 Cell Nuclei

Observer/OLGA	Correlation index (r^2)	Linear regression
OLGA versus Obs. A	0.97	$0.99 \times +20$
OLGA versus Obs. B	0.96	$1.02 \times +32$
Obs. B versus Obs. A	0.99	0.97×-7

rithms (e.g., 23), or even manually at any point within the wide valley separating the two clusters.

Another example of applying PCA may be seen in Figure 6e, which illustrates a tissue section image containing a fewer number of cells and its corresponding 1st PC with the proliferating cells enhanced (Fig. 6f). After PCA, the image contrast is greatly improved, as pixel data are projected along a line in which the values of the pixels are most spread.

However, in cases where the histogram of the 1st PC did not have a clear bimodal histogram, the approach described in the “Histogram Processing” section was applied for selecting an appropriate threshold value. An example is given in Figure 7b, illustrating the 1st PC of the histological image shown in Figure 7a, which exhibits a low staining quality due to the uneven expression and staining of the proliferation marker by many cells across the tumor section. The generated image enhances the objects of interest to some extent, but clearly not as much as in the images of Figure 6. This may also be seen from the image histogram in Figure 7c, which presents a rather unimodal shape, denoting that proliferating cells are enhanced, but not as much as to form a second distinct peak that would make them more easily detectable. After applying the aforementioned empirical rule, an appropriate threshold is selected, as indicated by the arrow, separating effectively the proliferating cells (see also Fig. 8b).

Comparison of the PCA-Based Method with Other Thresholding Techniques and Manual Counting

The proposed PCA-based algorithm was compared with five common threshold selection techniques that have been used widely by many researchers for similar cell segmentation purposes (5,32,33), since they hold the advantage of being fast and simple to implement, as discussed by others (6). These thresholding techniques were: method A, *iterative selection* (24); method B, *entropic thresholding* (22); method C, *Otsu's method* (23); and method D, *fuzzy sets* (21). All of these methods are based on different clustering criteria for applying a threshold, which in this study's application would discriminate the two classes corresponding to proliferating cell nuclei and hematoxylin-labeled cells together with tissue background.

To evaluate the outcome of the different algorithms studied, the figure of certainty (FOC) measure was used as

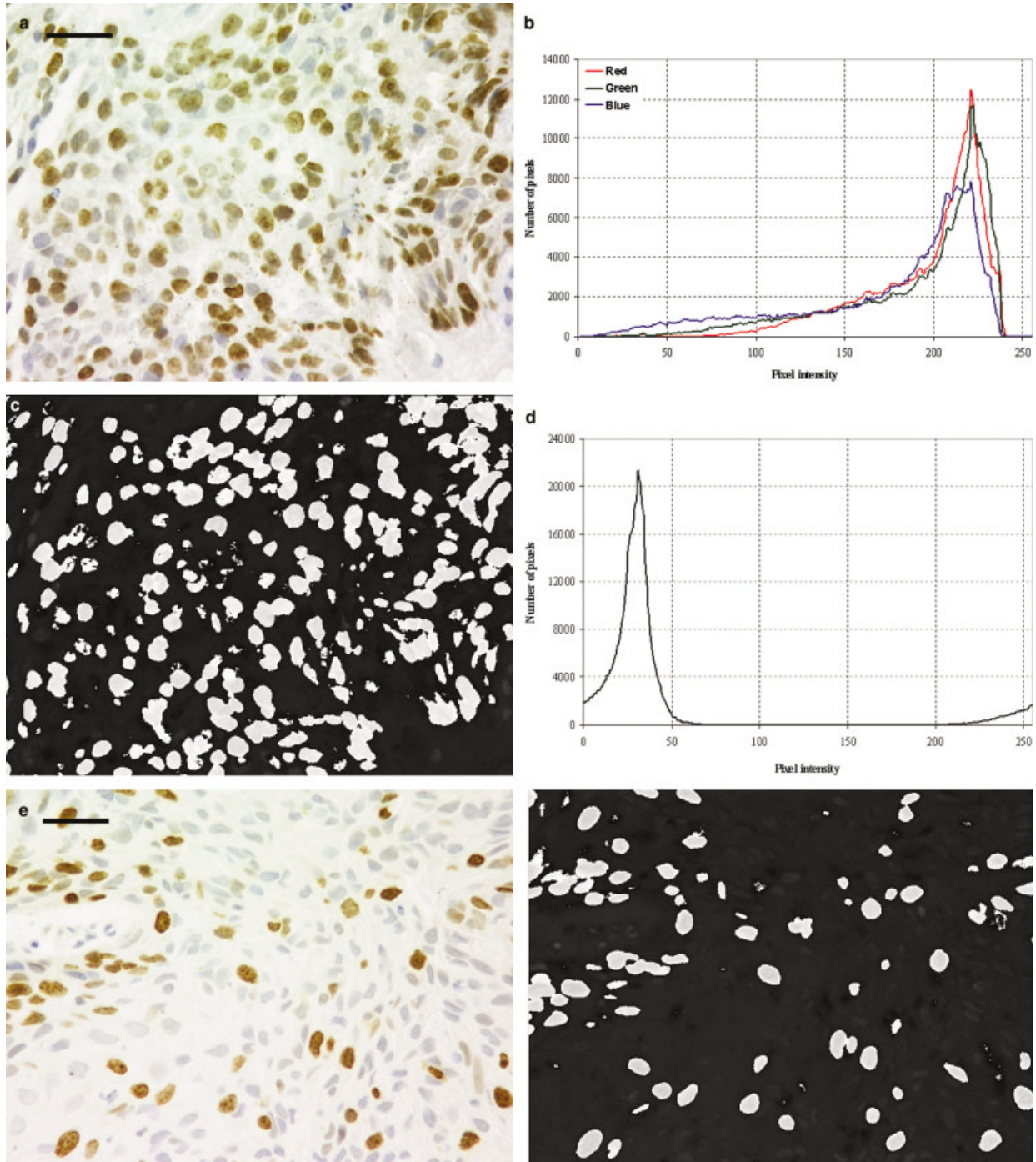


FIG. 6. **a** and **b**: A typical large-scale tissue section image and the histograms of its R, G, and B bands, all of which exhibit a rather unimodal shape. **c** and **d**: The 1st PC (after performing PCA) of the original color image shown in (a) and its gray-level histogram with a clear valley in between the two major pixel populations. **e** and **f**: Another histological image with its corresponding 1st PC, where positively stained cells are also greatly enhanced. Bar = approximately 30 μm .

described in Strasters and Gerbrands (34). FOC is given essentially by the same equation as FOM (Eq. 5), but now N is the number of objects detected in the image by a particular method, and d_i is replaced by the normalized color error e_i associated with each cellular object i found by the algorithm

$$e^2 = \frac{1}{f}(e_R^2 + e_G^2 + e_B^2) = \frac{1}{f} \left(\sum_{j=R,G,B} \sum_{k=1}^{k=N} (g_{jk} - \bar{g}_j)^2 \right) \quad (6)$$

where e_R^2 , e_G^2 , e_B^2 are the squared errors at each color band R, G, and B, respectively; g_{jk} is the gray value of the k th

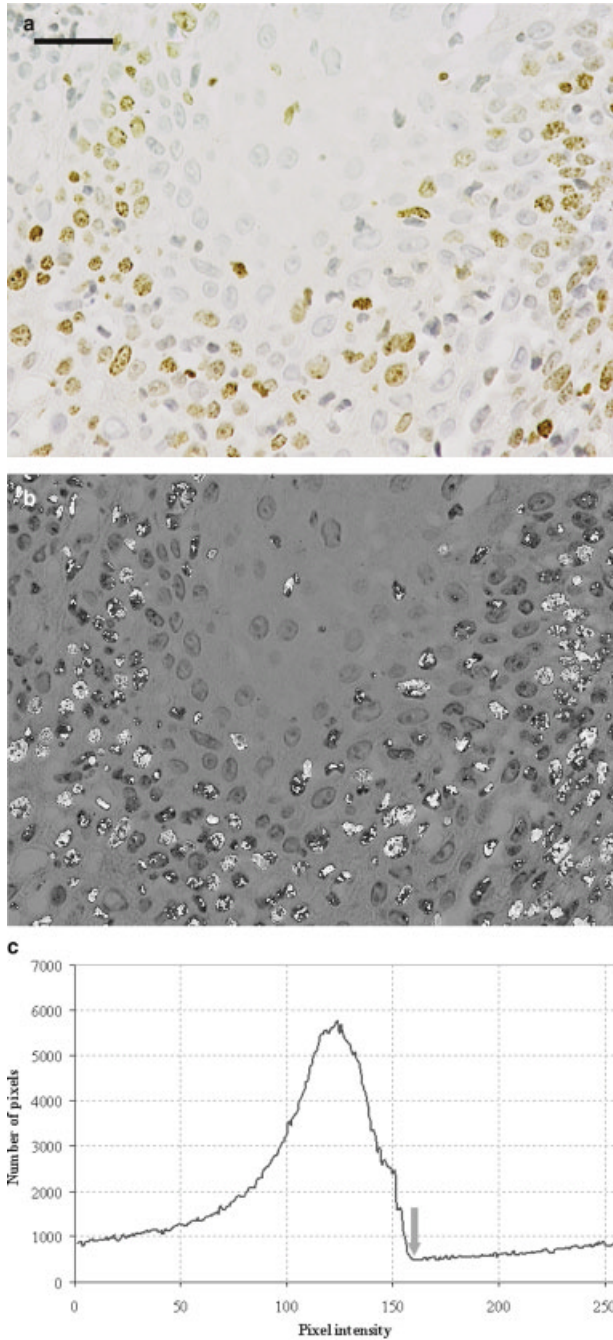


FIG. 7. Typical example of a histological image with low quality of staining (a), its 1st PC (b), and its histogram (c). The elevation on the right of the histogram corresponds essentially to the originally proliferation-stained cells (shown as light gray in b). The gray arrow on the histogram indicates the desirable cutoff gray-level value, which was detected using the threshold selection method described in the “Histogram Processing” section. Bar = approximately 30 μm .

pixel at the j th band; and \bar{g}_j is the mean value at band j of a sample containing various proliferating cells extracted from each image being evaluated. Note also that the overall error value is divided by f , which is a scaling factor used to normalize e^2 in the range [0, 1].

FOC indicates a measure of fit of the color properties of the objects extracted, using a sample of proliferating cell nuclei, with their member image elements. However, there is a possibility that an algorithm may exclusively find some but not all the stained cell nuclei in an image. This would result in a high FOC, but would inevitably lead to a false negative error. To take this type of error into account, a different set of experiments was also conducted, involving manual counting. Specifically, two different observers marked the proliferating cells in 10 full-scale test images, containing 40–500 (average 150) stained nuclei, and the individual counts were used as the gold standard. Each of the thresholding algorithms, along with the PCA-based method, was then applied separately, in order to detect the proliferating nuclei, followed by some standard morphological procedures to obtain solid objects and reject small-size particles.

Table 2 summarizes the threshold values generated after applying each of the four thresholding algorithms in the test images studied. The blue component from each original color image was chosen in that case, since it was found to present the best contrast between stained nuclei and histological background. For comparison, the FOC mean values are also shown for each method, including PCA. From this table it can be seen that the first three algorithms generate similar threshold values, leading also to similar FOC values. Method D appears to find a rather low threshold value, leading consequently to a higher FOC, although the difference does not seem to be significant, mainly due to the limited dynamic range of FOC measures for assessing the best and worst performances. However, it was observed that all the objects detected by this method corresponded to proliferating cells, but at the same time, the algorithm failed to detect many other positive cells, leading to a large false negative error. Finally, the FOC for the PCA-based method is very close to those of methods A, B, and C. The threshold values applied in the 1st PC of the color image are not shown since the latter was different than the blue component used as input to the other algorithms.

In the second set of experiments, cell counts generated by each method were compared to the manual counts of two different observers, using the same 10 test images as before. To substantiate these results, the average percentage error between the manual counts of each observer and each of the five methods tested was calculated. Table 3 shows these percentage cell count errors and also the average error between the two different observers (interobserver error). Clearly, PCA combined with histogram processing shows the best performance with error rates (4–7%), comparable to the person-to-person comparison (4–5%). All other methods perform less well, with the worst being method D, although its FOC was the highest, suggesting an underestimation of the actual number of cell nuclei. As noted earlier, this algorithm tended to find a rather low threshold, resulting in a large fraction of positive cells incorrectly identified as negative.

Finally, Figure 8 illustrates the result of proliferating cell nuclei detection on four large-scale histological images with variable degrees of staining, using the PCA-based

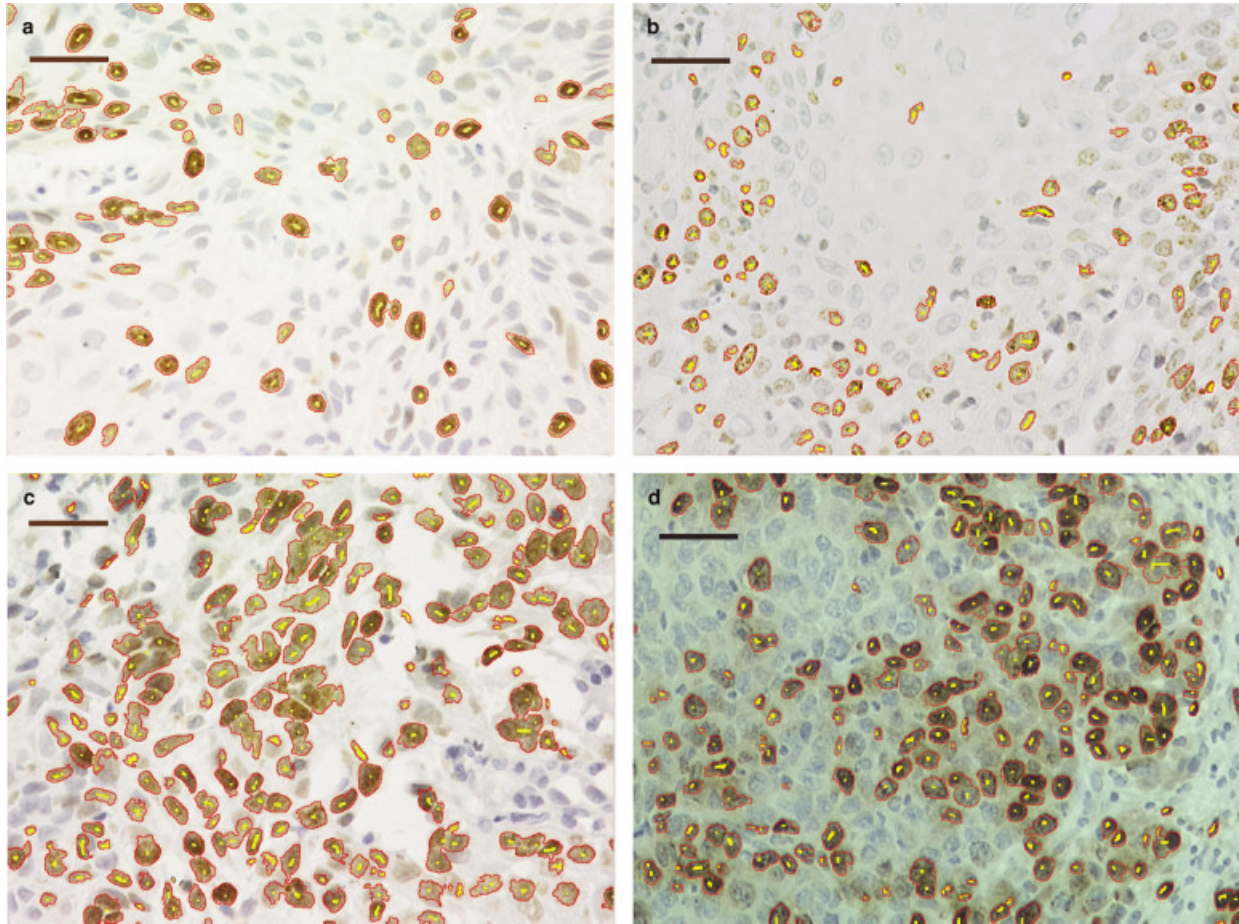


FIG. 8. Segmentation results on four histological images using the PCA algorithm, combined with histogram processing of the generated 1st PC. Again, cell nuclei borders are marked with red, whereas their centers are shown in yellow. **a** and **b**: Essentially those images shown in Figures 6c and 7a, respectively. Bar = approximately 30 μm .

segmentation algorithm. Again, cell borders are marked with red, whereas individual nuclei within clusters are marked with yellow, which are essentially the identified maxima after distance mapping. Figure 8b illustrates the outcome of proliferating cell detection on the original

image shown in Figure 7a, whereas Figure 8c and d show two more output images containing a larger number of nuclei. The image in Figure 8d was derived from a mouse adenocarcinoma and was used as an example of different tumor morphology. It can be seen that in all images the

Table 2
Threshold Values and Average FOC Measures Over 10 Large-Scale Histological Images for the Five Different Methods

Images	(A) Iterative Selection	(B) Entropic Thresholding	(C) Otsu's Method	(D) Fuzzy sets	(E) PCA with histogram
1	154	145	156	121	NA
2	183	176	184	119	NA
3	149	134	151	131	NA
4	160	163	163	129	NA
5	148	166	149	134	NA
6	149	140	151	129	NA
7	155	146	156	129	NA
8	141	135	140	109	NA
9	179	184	188	139	NA
10	136	128	133	110	NA
FOC	0.6235	0.6274	0.6249	0.6440	0.6263

NA, not applicable.

Table 3
Validation Studies on Proliferating Cell Counting*

	Observer A	Observer B
(A) Iterative selection	9.5	15.8
(B) Entropic thresholding	20.7	20.0
(C) Otsu's method	18.5	25.4
(D) Fuzzy sets	36.7	29.2
(E) PCA with histogram processing	7.3	4.4
Observer A		3.7
Observer B	5.0	

*The numbers represent percentage cell count errors (averages over 10 test images), between the manual counts of each observer and each of the five methods tested. For comparison the inter-observer errors are also shown. The cell counts of each observer was taken separately as the 'gold standard' for normalizing the percentage errors shown in the rows of each of the two columns.

proliferating cells are identified successfully, with the fraction of objects detected incorrectly as positively stained nuclei being low.

DISCUSSION

In this study the problem of computer-based detection and segmentation of cell nuclei in large-scale histological images was investigated. The main drive of the presented research work emanated from the requirement of a robust and automated method for assessing the proliferating activity of tumors in order to be able to assess changes after radiotherapy, or chemotherapy, and in general to derive quantitative information regarding the tumor morphology.

In the field of histology the simplest way to obtain proliferation information is to stain tumor sections with proliferation-dependent antibodies, such as the Ki-67 and cyclin A employed in this study. The fractions of stained cells are related to different aspects of the proliferative fraction and are useful to rank tumors such that patients could be selected for an appropriate treatment schedule. However, the procedures currently in clinic employ manual cell counting or semiquantitative assessment, both of which are tedious, laborious, and subjective.

To obtain knowledge of cellular populations and architecture in a tumor region a technique has to be developed that is able to discriminate the proliferation-labeled cell nuclei from others, and then measure their fraction, or find spatial relations with other biological structures (see Loukas (12)). For the purposes of this research study, such algorithms had to be suitable for tissue sections stained both with hematoxylin and with proliferation markers. There is currently no commonly acceptable method for this task, especially for large-scale images with complex appearance containing several hundred cells. The method proposed was based on detecting the overall number of cells irrespective to their stain, using edge detection, and then the number of proliferating cells using a PCA-based method with histogram analysis. This is a new approach to this problem, as most of the algorithmic approaches reported in the literature focus on gray-level thresholding

either made interactively or based on empirical selection criteria.

Since the borders of the cells are the only prominent features for discriminating cellular structures regardless of their biological marker, the methodology of edge detection was employed. Edge detection provides significant merits such as low computational cost, something essential when one deals with large-scale images, and minimum user interaction. It does not also assume that the gray intensities of the cells have a specific form, which is usually a prerequisite for other algorithms employing histogram thresholding. LoG was modified leading to OLGA, as the former was found to generate a fuzzy set of edgels, which were extremely difficult to connect, resulting in erroneous segmentation. The adequacy of the latter for the problem of cell nuclei detection was demonstrated with various validation experiments, including comparison with manual counting.

The next goal was to assess tissue areas of high growth activity by detecting those cells stained with a proliferative marker. This would allow the extraction of important clinical parameters that can be correlated with tumor progression and treatment outcome. A multistage algorithm is proposed that is almost parameter-free and uses PCA at its outset in order to generate weighted linear combinations of RGB, with large discriminative power. This has the advantage of producing an image where the cells of interest are greatly enhanced over all other structures and their segmentation becomes easier. Unlike most studies found in the literature, which are limited to quantification of staining by empirically selected color transformations and thresholds, the proposed method does not assume that the spectral characteristics of the image acquisition system are matched with the absorption spectra of the stains. Alternatively, it identifies a linear transformation of the original RGB color space, such that the three axes of the new coordinate system coincide with the directions of the three largest spreads of the point distribution. The 1st PC has the greatest contrast and contains the maximum possible information conveyed by a single band of the color image. Furthermore, the generated linear combination could remain the same for all images originating from the same slide, provided the spectral characteristics of the stain do not vary significantly from image to image, something that reduces remarkably the overall computational cost. Various experiments on stained cell counting showed that the cell count error approached the person-to-person variability, while comparison with several gray-level thresholding methods revealed the advantage of combining color information prior to histogram analysis.

In conclusion, automated cell counting in complex large-scale histological images could be applied in routine practice using algorithms based on second-order edge detection and PCA with thresholding. With the noisy histological data encountered in clinical practice, it seems unlikely that fast and automated cell detection can be achieved using a priori information regarding the geometrical characteristics, or gray-level properties of the cell

nuclei. However, the proposed algorithms provide several benefits, such as speed of analysis (~6 s on a modern computer for the combination OLGA-PCA), consistency, and automation, and they are considerably faster than human observation (approximately 30 times faster). The automated counter is also consistent, as it produces the same counts for a given digitized microscopy field, something that is not true for its human counterpart. The aforementioned algorithms have also been integrated into a specific problem-designed image analysis software (Cell-ID, see Loukas (12)) for enhancing the quantitative analysis of histological sections, especially in cases of dual-stained tumor tissue.

ACKNOWLEDGMENTS

C. Loukas was funded by a postgraduate scholarship from the Cancer Research Campaign (grant STU 045/001). The authors thank Mrs. Locke for development of the image acquisition software, Mr. Newman for assistance with hardware, Mrs. Daley for assistance with cell counting, and Dr. Barber for comments during the early course of this study.

LITERATURE CITED

- Green JR. Parallel processing in a pattern recognition based image processing system: the Abbott ADC-500 differential counter. *Proc IEEE Conf Pattern Recognition Image Processing* 1978;31:492-498.
- Bartels PH, Wied GL. A high resolution prescreening system for cervical cancer. The automation of uterine cancer cytology. *Tutorials of Cytology*, Chicago, IL, University of Chicago Press. 1976:144.
- Watanabe JS, the CYBEST Group. An automated apparatus for cancer prescreening: CYBEST. *Comput Graphics Image Process* 1974;3:350-358.
- Francis IM, Adeyanju MO, George SS, Junaid TA, Luthra UK. Manual versus image analysis estimation of PCNA in breast carcinoma. *Anal Quant Cytol Histol* 2000;22:11-16.
- Weaner JR, Au JLS. Application of automatic thresholding in image analysis scoring of cells in human solid tumours labeled for proliferation markers. *Cytometry* 1997;29:128-135.
- Lehr HA, Van der Loos CM, Teeling P, Gown AM. Complete chromogen separation and analysis in double immunohistochemical stains using Photoshop-based image analysis. *J Histochem Cytochem* 1999; 47:199-225.
- Mouroutis T, Roberts AJ, Bharath AA. Robust cell nuclei segmentation using statistical modeling. *Bioimaging* 1998;6:79-91.
- Sjostrom PJ, Frydel BR, Wahlberg LU. Artificial neural network-aided image analysis system for cell counting. *Cytometry* 1999;36:18-26.
- Lotayef M, Wilson GD, Daley FM, Shouman T, Awwad H. Aberrant expression of cyclin A in head and neck cancer. *Br J Cancer* 2000; 83:30-34.
- Pal NR, Pal SK. A review on image segmentation techniques. *Pattern Recognition* 1993;26:1277-1294.
- Marr D, Hildreth EC. Theory of edge detection. *Proc R Soc London* 1980;B207:187-217.
- Loukas CG. Quantitative image analysis of biological factors influencing radiotherapy. Ph.D. thesis, University College London, University of London, UK, 2002.
- Huertas A, Medioni G. Detection of intensity changes with subpixel accuracy using Laplacian-Gaussian masks. *IEEE Trans Pattern Anal Machine Intelligence* 1986;8:651-664.
- Danielsson PE. Euclidian distance mapping. *Comput Graphics Image Process* 1980;14:227-248.
- Loukas CG, Wilson GD, Vojnovic B, Linney A. Automated segmentation of cancer cell nuclei in complex tissue sections. *SPIE Biomonitoring Endoscopy Technol* 2000;4158:188-198.
- Malpica N, Solorzano CO, Vaquero JJ, Santos A, Vallcorba I, Garcia-Sagredo JM, del Pozo F. Applying watershed algorithms to the segmentation of clustered nuclei. *Cytometry* 1997;28:289-297.
- Ruifrok AC. Quantification of immunohistochemical staining by color translation and automated thresholding. *Anal Quant Cytol Histol* 1997;19:107-113.
- Smolle J. Optimization of linear image combination for segmentation in red, green and blue images. *Anal Quant Cytol Histol* 1996;18:323-329.
- MacAulay C, Tezcan H, Palcic B. Adaptive color basis transformation. An aid in image segmentation. *Anal Quant Cytol Histol* 1989;11:53-58.
- Petrou M, Bosdogianni P. Image processing. The fundamentals. West Sussex, Chichester, UK: Wiley & Sons Ltd. 1999:136-144.
- Huang LK, Wang MJ. Image thresholding by minimising the measures of fuzziness. *Pattern Recognition* 1995;28:41-51.
- Kapur JN, Sahoo PK. A new method for gray-level picture thresholding using the entropy of the histogram. *Comput Vision Graphics Image Process* 1985;29:273-285.
- Otsu N. A threshold selection method from gray-level histograms. *IEEE Trans Syst Man Cybern* 1979;9:62-66.
- Thruswell HJ. Comments on picture thresholding using an iterative selection method. *IEEE Trans Syst Man Cybern* 1979;9:311.
- Adiga PSU, Chaudhuri BB. Region based techniques for segmentation of volumetric histopathological images. *Comput Methods Programs Biomed* 2000;61:23-47.
- Ong SH, Jin XC, Jayasooriah, Sinniah R. Image analysis of tissue sections. *Comput Med Biol* 1996;26:269-279.
- Veropoulos K, Learmonth G, Campbell C, Knight B, Simpson J. Automated identification of Tubercle Bacilli in sputum. *Anal Quant Cytol Histol* 1999;21:277-282.
- Canny J. A computational approach to edge detection. *IEEE Trans Pattern Analysis and Machine Intelligence* 1986;8:679-698.
- Pratt WK. *Digital image processing*. New York: John Wiley & Sons Ltd. 1978:65-71.
- Venkatesh S, Kitchen LJ. Edge evaluation using necessary components. *Comput Vision Graphics Image Process* 1992;54:23-30.
- Zhang YJ. Evaluation and comparison of different segmentation algorithms. *Pattern Recognition Lett* 1997;18:963-974.
- Demirkaya O, Cothren RM, Vince DG, Cornhill JF. Automated identification of stained cells in tissue sections using digital image analysis. *Anal Quant Cytol Histol* 1999;21:93-102.
- Wu HS, Gil J, Barba J. Optimal segmentation of cell images. *IEEE Proc Vision Image Signal Process* 1998;145:50-56.
- Strasters KC, Gerbrands JJ. Three-dimensional image segmentation using a split, merge and group approach. *Pattern Recognition Lett* 1991;12:307-325.